ISSN 2522-9400 **European Modern Studies Journal** Vol 8 No 2
available at www.journal-ems.com
DOI: 10.59573/emsj.8(2).2024.45

High-Resolution Precipitation Mapping for Morocco: Integrating Orographic and Geographic Influences

Abdelmonaim Okacha[1]*, Adil Salhi[1], Mounir Bouchououu[1], Kamal Lahrichi[2], Hamid Fattasse[2], Kamal Abdelrahman[3]
[1]Geography Department, Abdelmalek Essaadi University, Martil, B.P. 210, Morocco
[2]Geography Department, Sidi Mohamed Ben Abdellah University, Fez, 30000, Morocco
[3]Geology Department, King Saud University, Riyadh, 11451, Saudi Arabia

Abstract. Morocco's mountainous regions play a crucial role in shaping its precipitation patterns, influencing everything from water resources to agricultural potential. However, accurately mapping precipitation in such complex terrain is challenging for traditional methods. This study proposes a model that incorporates both topographic and geographic features and prevailing weather patterns to create more accurate maps of average annual precipitation across Morocco. What sets this model apart is its ability to determine the direction of prevailing weather circulation and incorporate geographic and topographic parameters that influence precipitation patterns. Using data from 1965 to 2010, the model estimates an average annual rainfall of 206.4 mm, equivalent to 146.6 billion cubic meters per year, with a terrain aspect deviation to the dominant moisture flux direction set at 280 degrees. This approach is particularly valuable in regions with limited climate data networks, as it leverages existing information to fill in the gaps. By providing more accurate precipitation maps, this model can be a valuable tool for environmental modeling, water resource management, and agricultural planning in Morocco.

Keywords: precipitation, mapping, interpolation method, orographic and geographic effects, weather circulation

Introduction

Precipitation is widely acknowledged to be a significant component influencing environmental and hydrological processes and thus serves as an essential input parameter in several models and applications designed for forecasting and investigating these processes (Alsafadi, Mohammed, Mokhtar, Sharaf, & He, 2021; Beck et al., 2019; Di Piazza, Conti, Noto, Viola, & La Loggia, 2011; Prakash, 2019; Wei et al., 2023). It is used as a key input variable in various models, including hydrological, climate, agricultural, and weather forecasting models (Du, Wang, Zhu, Lin, & Zhong, 2022; Fu, Sonnenborg, Jensen, & He, 2011; Jin, Chen, Wu, Song, & Xia, 2021). To ensure a solid foundation for such models, it is imperative to consider the spatial distribution of precipitation and account for the spatial differences arising from various influencing factors (Crochet et al., 2007; Jeniffer, Su, Woldai, & Maathuis, 2010). For instance, climate models require accurate identification of spatial disparities in precipitation patterns in order to ascertain future trends. The climate fluctuations and changes has become realistic and are weighing on the economies of many countries (Pichura, Potravka, & Barulina, 2023) (particularly in the MENA regions which are characterized by strong climate fluctuations and scarce rainfall), making precipitation distribution studies particularly critical (Giovanis & Ozdamar, 2022; Waha et al., 2017).

Extensive and diligent research has been undertaken in the realm of precipitation mapping across diverse global regions. These comprehensive studies aim to gain a profound understanding of the intricate challenges and promising opportunities associated with mapping

* Corresponding Author

precipitation in various geographical landscapes. A wide array of techniques has been employed, ranging from traditional ground-based observations to modern methodologies such as satellite and radar measurements, Thiessin Polygons (Barbulescu, 2016), Least Square Regression (Shu, Wang, & Xiong, 2007), Inverse Distance Weighting (Tan et al., 2021), Kriging (Bostan, Heuvelink, & Akyurek, 2012; Chang, 1991; Seo, Kim, & Singh, 2015; Symeonakis, Bonifaçio, & Drake, 2009; Verdin, Rajagopalan, Kleiber, & Funk, 2015), Splines (Hofierka, Parajka, Mitasova, & Mitas, 2002), and Local and Global Polynomial Interpolation (Gilewski, 2021). These techniques employ mathematical algorithms to estimate rainfall at unsampled locations based on observations from nearby points (Ly, Charles, & Degré, 2013).

Spatial interpolation enables the creation of high-resolution precipitation maps with commendable accuracy (Camera, Bruggeman, Hadjinicolaou, Michaelides, & Lange, 2017). However, its efficacy relies on the quality and distribution of observed data as well as the interpolation technique employed. It is worth noting that while spatial interpolation considers spatial relationships between observed points, it often fails to account for significant orographic variations (Bookhagen & Strecker, 2008). Therefore, numerous studies have demonstrated that incorporating additional explanatory factors yields more accurate precipitation estimates compared to relying solely on interpolation methods. Factors such as radar imagery, latitude, distance from the coast, and orographic effects, including altitude and terrain aspect deviation from the dominant moisture flux direction, have proven instrumental in enhancing precision (Alsafadi et al., 2021; Daly, Neilson, & Phillips, 1994; Daly, Slater, Roberti, Laseter, & Swift Jr, 2017; Guan, Wilson, & Makhnin, 2005; Gundogdu, 2017; Hofierka et al., 2002; Lloyd, 2005; Lloyd, 2010; Ninyerola, Pons, & Roure, 2007). Consequently, integrating these explanatory variables as independent factors into precipitation estimation models offers a viable approach for precise assessment of precipitation amounts. The strong correlation between these parameters and the spatial distribution of precipitation makes this approach particularly valuable in areas characterized by challenging geography and topography (Basist, Bell, & Meentemeyer, 1994; Daly et al., 1994; Danard, 1976; Diodato & Ceccarelli, 2005; Vidal P & Varas, 1982).

In line with this rationale, the ASOADeK model (Auto-Searched Orographic and Atmospheric Effects Detrended Kriging) demonstrated its superior performance in mapping monthly precipitation in northern New (Guan et al., 2005). This approach involved the utilization of gauge precipitation data and the application of a multivariate linear regression method to examine both local and regional climatic parameters. Comparisons with precipitation kriging and precipitation-elevation cokriging methods revealed that the model, by fully accounting for atmospheric and orographic information, achieved higher levels of accuracy.

In a similar vein, the PRISM (Parameter-elevation Regressions on Independent Slopes Model), developed by Oregon State University (Daly et al., 2008; Daly, Taylor, & Gibson, 1997), has demonstrated its performance in generating high-resolution precipitation maps. By combining elevation data with statistical models, PRISM has been extensively utilized in various studies to map precipitation across different spatial and temporal scales (Daly et al., 2008; Jeong, Ahn, Lee, Shim, & Jung, 2020).

Both models underscored the importance of including explanatory variables in precipitation interpolation, leading to improved results compared to methods relying solely on gauge precipitation data. However, it is crucial to consider the scale at which topography influences precipitation during the application of these models (Meersmans et al., 2016). Indeed, the inclusion of explanatory variables in precipitation interpolation enables a more comprehensive understanding of the intricate interplay and spatial variations among climatic, atmospheric, and topographic factors that influence the distribution of precipitation. Moreover, considering the matter of scale is crucial when examining the effects of topography on precipitation. The influence of topographic features such as mountains, valleys, or coastal areas on precipitation patterns can vary depending on the size and geographic characteristics of the region under investigation, creating distinct microclimates which have a significant impact on the distribution of precipitation.

With this in mind, incorporating and accounting for scale-dependent influences in precipitation interpolation models becomes crucial to generate more precise estimates and enhance the overall reliability of the mapping process. It is essential to consider the scale at which topography influences precipitation, as the effects can vary based on the size and geographic characteristics of the region under study. Various topographic features, such as mountains, valleys, and coastal areas, create distinct microclimates that significantly impact precipitation patterns. Fine-tuning the modeling approach at the appropriate scale ensures reliable and precise precipitation estimates, with implications for water resource management, climate studies, and disaster preparedness.

In this study, an innovative model was developed, employing an advanced interpolation technique that integrated the sine function of the deviation of terrain aspect to the dominant moisture flux direction. The model also incorporated the scale at which topography influenced precipitation, latitude effect, and distance from the coast. These four factors aimed to provide a comprehensive and accurate understanding of precipitation dynamics in complex terrains. Rigorous testing and validation were conducted to assess the effectiveness of the model, with the ultimate objective of advancing our knowledge of the intricate relationships between atmospheric conditions, topography, and precipitation patterns.

The application of such techniques in data-scarce areas holds significant importance, particularly in understanding the spatial distribution of precipitation. Morocco, being representative of such data-scarce regions, was selected as a case study in this research. Notably, Morocco encompasses a wide range of distinct aspects pertaining to the main factors that influence precipitation distribution, including scale topography, terrain aspect, distance to the coast, and latitude. Therefore, it serves as an ideal candidate for investigating the effectiveness of the proposed approach in capturing the intricate relationships among these influential factors. By conducting the case study in Morocco, this research aims to contribute valuable insights into precipitation dynamics in data-scarce areas, ultimately enhancing our understanding of the spatial patterns and improving the availability of reliable precipitation information.

Material and Methods

Study Area

The research focuses on the northwestern region of Africa, stretching from the Atlantic Ocean to the Mediterranean Sea (Fig. 1). Encompassing longitudes 0°-17° W and latitudes 20°-36° N, the area spans 710,850 km². Its topography and strategic location yield diverse bioclimatic conditions, featuring six climate zones: Mediterranean, Saharan, arid, semi-arid, humid, perhumid, and subhumid (Benabid, 2000).

The annual rainfall varies significantly across the region. From the humid context in the Rif Mountain in the North, it decreases to Saharan conditions in the south, ranging from less than 100 mm in the Sahara to over 1700 mm in the mountainous areas on the west side of the Rif Mountains.

The agricultural sector is integral to Morocco's economy, employing 40% of the population and contributing 15% to 20% to the GDP (AAD, 2015). Beyond its economic significance, agriculture plays a pivotal role in food security, export, and cultural preservation. However, the sector faces challenges due to precipitation fluctuations impacting productivity (Benyoussef et al., 2024; Chanyour, El Achari, Hanchane, Obda, & Kessabi, 2024). This has led to rural-urban migration and migration to Europe (Okacha, Salhi, Arari, Elbadaou, & Lahrichi, 2023; Salhi et al., 2020; Salhi, Vila Subirós, & Insalaco, 2022).

Numerous studies have addressed these challenges, focusing on rainfall variability and trends (Ouharba, Mabrouki, & Triqui, 2024; Salhi et al., 2019). Precipitation aggressivity is vital for environmental and hydrological models, especially those assessing soil loss. Despite its importance, the spatial distribution of rainfall in agricultural planning has been underexplored, warranting further investigation.

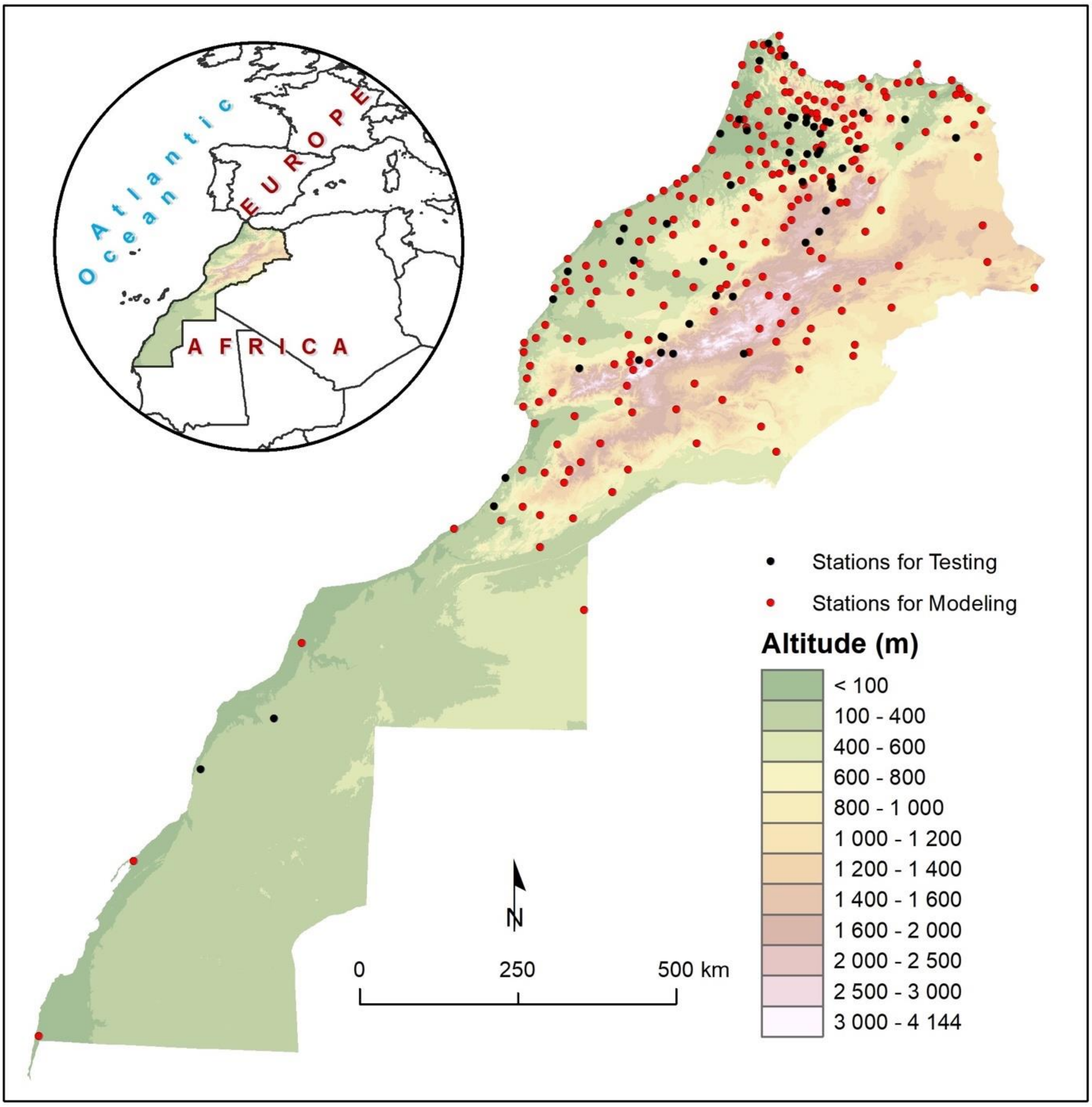

Figure 1. Location of the study area and stations used

Climate, Geographical, and Topographical Data

The precipitation data utilized in this study was sourced from reputable and authoritative entities within the field, specifically the Hydrographic Basin Agencies and the National Meteorological Directorate (DMN). These organizations are recognized as authoritative sources for reliable and comprehensive precipitation data, ensuring the credibility and integrity of the dataset used for analysis in this research. In addition to these primary data sources, supplementary information was gathered through an extensive literature review encompassing scientific articles, research reports, and relevant publications. The dataset utilized in this research encompasses mean monthly precipitation values recorded at 288 meteorological stations from 1965 to 2010. Out of these stations, 234 were selected for the purpose of modeling, while the remaining 54 stations were designated for testing and validation purposes (Fig. 1). The utilization of a substantial number of stations for modeling and testing further strengthens the statistical robustness and generalizability of the study's findings. This rigorous approach ensured a complete and reliable data set for the study. To ensure the reliability and validity of the results, the data collected were subjected to rigorous quality control procedures, including data cleaning, validation and verification. Additionally, statistical analysis techniques were applied to assess data consistency and identify any outliers or potential anomalies.

The present study employed a rigorous approach involving corrections and verifications to mitigate potential errors associated with topographical data and geographical coordinates provided by administrative authorities. These processes were facilitated by referencing Open Street Map (OSM) and Google Map, which serve as reliable sources for accurate and up-to-date spatial information. By leveraging these supplementary resources, the study ensures the reliability and validity of the topographical and geographical data used in the modeling.

The topographic data utilized in this study was obtained from Aster GDEM Version 2 digital terrain model (Tachikawa et al., 2011). The geographic coordinates (x, y) were extracted from the Digital Elevation Model (DEM). Initially, the 30 m DEM underwent a smoothing process using ArcMap's spline and Natural Neighbor tools. Prior research conducted by Meersmans et al. (2016) demonstrated that the smoothed DEM, at scales of 8.1 km for h1, 90 km for h2, and 30.6 km for S, had significant implications. Additionally, Daly et al. (2017) emphasized the importance of a smoothed DEM at scales ranging from 5 to 10 km in assessing the influence of elevation on precipitation within a mountainous watershed.

In the present study, the investigation of the optimal effects of Z2 altitude on precipitation revealed that the most substantial impacts were observed at scales of 30 km and 50 km for sin(s), while for Z1, a scale of 1 km yielded the most significant results (Fig. 2). These findings contribute to the understanding of the relationship between altitude and precipitation patterns, particularly in the context of the study area.

Interpolation Procedures

Numerous techniques and methodologies have been utilized in examining spatial precipitation patterns and their fluctuations across several research studies. Specifically, an assessment of the impact of topography and other covariates in elucidating these variations is among the most prevalent approaches employed to incorporate diverse variables, encompassing topographic and geographic factors, for the spatial modeling of precipitation and other climatic parameters utilizing Geographic Information Systems (GIS) tools.

In this study, the input variables for the model were carefully selected based on their significant influence on precipitation mapping. These input variables included the distance from the coast, Latitude, terrain elevation, and the deviation of terrain aspect to the dominant moisture flux direction (DTAMD) (Fig. 2c).

The distance from the coast was found to have a considerable impact on precipitation mapping (Mirás-Avalos, Mestas-Valero, Sande-Fouz, & Paz-González, 2009), particularly in Atlantic regions where atmospheric conditions differ from inland regions. Additionally, the effect of Latitude on precipitation was observed through the correlation between the amount of solar radiation received and the distribution of precipitation across the Earth's surface. Specifically, the study area showed a decrease in precipitation from lower latitudes (20 degrees) in southern regions to higher latitudes (36 degrees) in northern regions due to the reduction in solar radiation received at higher latitudes.

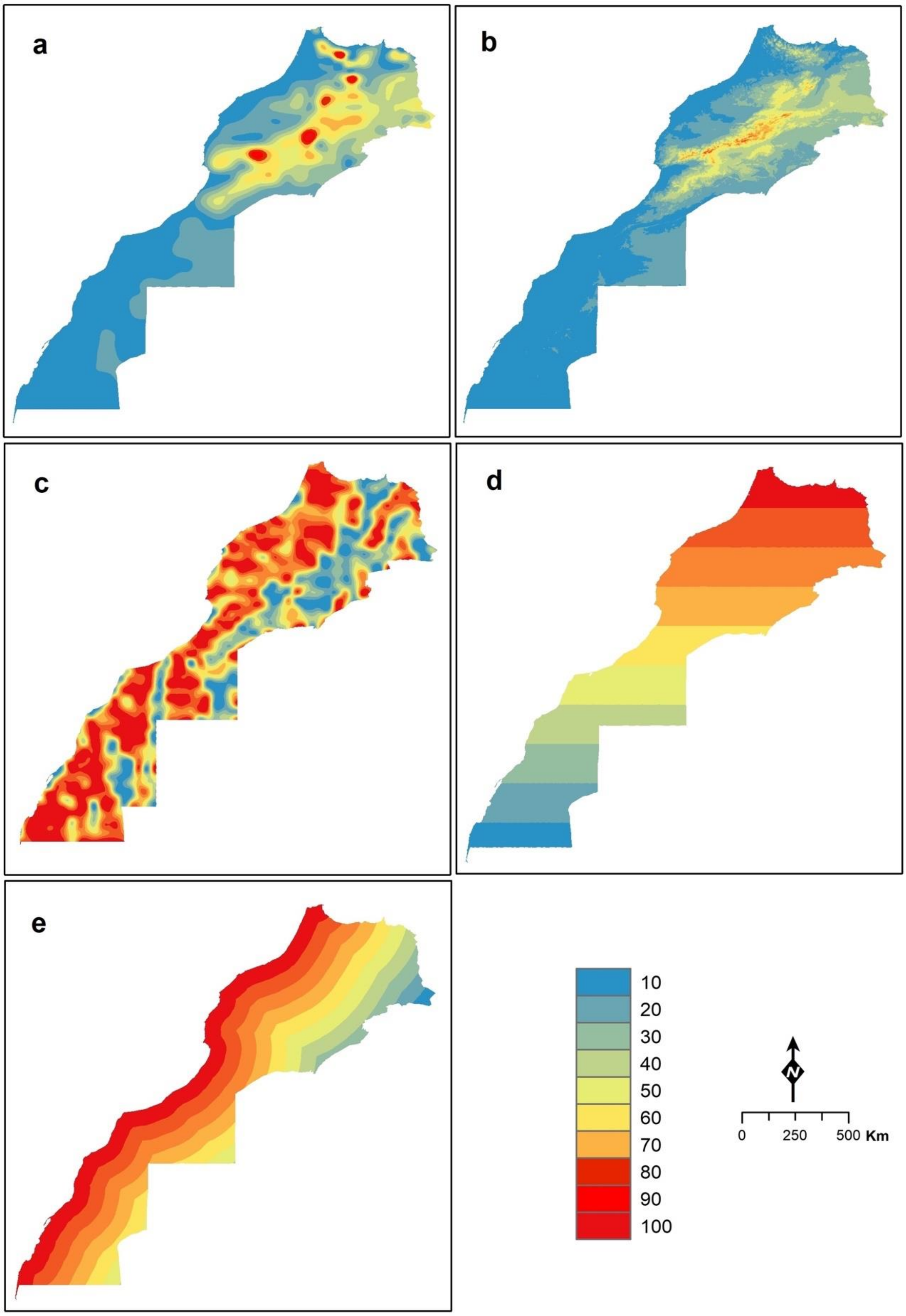

Figure 2. Maps of the explanatory variables: a: Z2 and b: Z1 represents the standardized height above sea level, c: sin(s) represents the function sin of the deviation of terrain aspect to the dominant moisture flux direction (DTAMD280°), d: Y represents the standardized Latitude and e: X represents the standardized distance from the coast. 10 represents the lowest standardized value, while 100 represents the highest standardized value.

Due to the influence of orographic effects, there is typically a strong correlation between the long-term average precipitation (P) and the elevation of the terrain (Z_1 and Z_2) (Guan et al., 2005). These orographic effects, such as the interaction between air masses and mountainous topography, play a significant role in shaping precipitation patterns. When moist air encounters a mountain range, it is forced to rise, cool, and condense, leading to increased precipitation on the windward side of the mountains, known as the orographic effect or orographic lifting. The amount of precipitation can vary significantly based on the characteristics of the mountain range, such as its height, slope, and orientation to prevailing winds. Additionally, mountain ranges can produce rain shadows, which are areas with reduced precipitation on the leeward side of the mountains, as air masses lose their moisture on the windward side and descend on the leeward side, resulting in drier conditions.

The proposed model considers the distance from the coast, the Latitude, the altitude, and the relationship of moisture flux direction and terrain aspect as independent variables for precipitation estimates. In order to facilitate the analysis of the effects of each variable, all the independent variables are standardized where the values having maximum effects take 100 and those having weak effects take 0. In order that the effects of these independent variables are automatically deduced by regression multiple, they are explicitly introduced in the regression function (Eq. 1). The distance from the coast (X) and Latitude (Y) of the rain gauge stations are used to find the spatial gradient of atmospheric humidity. The elevation of the land above sea level (Z1) is used in this study, with a resolution of 1km. Since the terrain aspect effect works with the direction of moisture flow, they are included in a sine, sin (s) function with a resolution of 30km, multiplying in altitude Z2 with a resolution of 50km. The aspect is defined as the direction of the orientation of the slope. The seven potentials deviation of terrain aspect to the dominant moisture flux direction (DTAMD) proposed are 130°, 160°, 175°, 190°, 205°, 220° and 250° (Table 2).

The average annual precipitation amount (P) in millimetres per year can be modeled using the equation:

$$P = a_1 X + a_2 e^{b \times y} + a_3 Z_1 + a_4 Z_2 \sin s \qquad \text{Eq. 1}$$

Where P: represents the dependent variable or the predicted value of average annual precipitation.

a_1X: Represents the linear relationship between the dependent variable P and the independent variable X, with a_1 being the coefficient for X. X represents the standardized distance from the coast, with a value of 100 denoting the coast of the Atlantic Ocean and decreasing towards inland regions, where the value is 0 for the innermost regions.

a_2e^{by}: Represents an exponential relationship between P and y, where e is the mathematical constant and a_2 and b are coefficients. Here, Y represents the standardized Latitude, with 0 denoting the southernmost point and increasing towards the North, where the value is 100.

a_3Z_1: Represents a linear relationship between P and Z_1, with a_3 being the coefficient for Z_1. Here, Z_1 represents the standardized height above sea level, with 0 denoting the lowest regions and increasing with altitude to a maximum of 100 for the highest regions.

$a_4Z_2\sin(s)$: Represents a combination of linear (Z_2) and trigonometric component (sin(s)) terms influencing P, with a_4 being the coefficient for Z_2. The variable Z_2 represents the standardized height above sea level, where its interaction with the sinus function of S is considered. S represents the deviation of terrain aspect to the dominant moisture flux direction (DTAMD), with 0 denoting the lowest values and 100 denoting the highest values.

The constant term c represents a fixed value affecting the model’s P.

The coefficients a1, a2, b, a3, a4, and c are parameters that determine the strength and direction of the relationship between the predictor variables and the response variable, providing insights into the factors influencing average annual precipitation (Table 1).

Table 1. Estimated values for the chosen model's parameters

Parameter	Value	95% Confidence interval	
a1	3.427	2.200	4.653
a2	19.434	15.31	23.855
b	0.037	0.033	0.041
a3	6.927	5.156	8.697
a4	10.200	8.578	11.822
c	-815.73	-932.16	-699.29

For every possible Deviation of Terrain Aspect to the Dominant Moisture Flux Direction (DTAMD), we selected a combination of X, Y, Z1, Z2, and sin(s) maps that resulted in the highest determination coefficient (including metrics such as MAE, MAPE, RMSE, MSE, R, and R^2) (Table 2). This allowed us to identify the most precise DTAMD. The chosen model output was then integrated with the corresponding X, Y, Z1, Z2, and sin(s) maps, with matching resolutions, to generate a 45-year average annual precipitation map for Morocco.

Residual Precipitation at the Gauge

The current study focuses on estimating precipitation and does not include the use of common spatial interpolation techniques. However, in the spatial analysis of proposed model residuals, spatial interpolation techniques have been used to create residual surfaces. These surfaces are combined with the model surface to produce a real surface that corrects for the inability of topographic and geographic variables to explain the complete spatial variation of precipitation.

To achieve this, various methods were analyzed, including Inverse Distance Weighting (IDW), Thiessin Polygons, Ordinary Kriging (OK) and Splines (Wang et al., 2014). Among these, Inverse Distance Weighting (IDW) is a deterministic interpolation method that calculates the values of unknown locations by averaging the values of known nearby locations, with the weight assigned to each known location based on its distance from the unknown location. The advantage of IDW in producing model residual map is that it is a relatively simple and straightforward method to implement, requiring only a few input parameters. IDW also has the advantage of being computationally efficient, making it suitable for use in large datasets. Additionally, IDW preserves local variations and can interpolate sharp gradients in the data, which is important for capturing small-scale spatial variation in precipitation. In this study, we applied Inverse Distance Weighting (IDW) method to produce residuals map.

Model Validation

The performance of a proposed model is commonly validated using cross-validation. In this study, the accuracy and robustness of our proposed model were evaluated using several performance metrics, including MAE, MAPE, RMSE, MSE, R and R^2. Cross-validation was performed for the proposed model, which was subjected to regression and IDW processes.

One commonly used metric is the Mean Absolute Error (MAE) (Eq.2), which calculates the average absolute difference between predicted and observed data. To express the MAE as a percentage of the actual value, the Mean Absolute Percentage Error (MAPE) (Eq.3) is used. In addition to MAE and MAPE, the Root Mean Squared Error (RMSE) (Eq.4) and Mean Squared Error (MSE) (Eq.5) are also widely used to evaluate prediction model accuracy. RMSE measures the standard deviation of the differences between predicted and observed values, while MSE calculates the average squared difference between the predicted and actual values. To assess the overall goodness of fit of a prediction model, the correlation between predicted and actual values can be measured using the R and R^2 metrics. These metrics are particularly useful in evaluating the predictive power of the model. This metric compares the variability of predicted values to the variability of observed data, and is particularly useful in assessing models used for prediction or forecasting. Here are the equations for the metrics mentioned:

$$MAE = \frac{1}{n} \sum_{i=1}^{n} |P_{pre} - P_{obs}| \quad \text{Eq.2}$$

$$MAPE = \frac{\sum_{i=1}^{n} \left| \frac{(P_{pre} - P_{obs})}{P_{obs}} \right|}{n} \times 100 \quad \text{Eq.3}$$

$$RMSE = \sqrt{\frac{1}{n} \sum_{i=1}^{n} (P_{obs} - P_{pre})^2} \quad \text{Eq.4}$$

$$MSE = \frac{1}{n} \sum_{i=1}^{n} \left(P_{pre} - P_{obs}\right)^2 \quad \text{Eq.5}$$

Where:
n is the total number of observations
P_{obs} represents the observed value
P_{pre} represents the predicted value
By using these metrics in combination, the accuracy and overall performance of prediction models can be evaluated in a clear and concise manner, enabling informed decisions based on empirical evidence.

The Best-Selected Model Comparison

The best-selected model was further compared to the Worldclim V2 and Chelsa V2.1 yearly mean precipitation products. The Worldclim V2 data was obtained by downloading the average yearly precipitation data from 1960 to 2000 spanning over 40 years, with a spatial resolution of approximately 1 km (Fick & Hijmans, 2017). Similarly, the Chelsa V2.1 data was downloaded, representing the average yearly precipitation data over 20 years from 1980 to 2010, with a spatial resolution of about 1 km (Karger et al., 2017). The data was estimated using advanced statistical methods to improve its accuracy and fill data gaps. Comparing the results obtained from the best model to these well-known and widely used precipitation datasets adds further credence to the accuracy and reliability of our model.

Results

Comparison of Models (without Residuals) according to DTAMD

Table 2 presents a comprehensive analysis of the ranking of models (without residuals) based on multiple evaluation metrics, including MAE, MAPE, RMSE, MSE, R, and R^2. Additionally, it includes angle values of the ‘‘deviation of terrain aspect to the dominant moisture flux direction’’ (DTAMD) to provide more insight into the impact of topography on model performance.

Table 2. Ranking of models (without adding the residuals) using MAE, MAPE, RMSE, MSE, R and R^2 with angle values of the ‘‘deviation of terrain aspect to the dominant moisture flux direction” (DTAMD)

Rank	DTAMD (°)	MAE	MAPE	RMSE	MSE	R	R^2
1	280	107.3136	47.29891	152.0985	23133.96	0.863	0.744762
2	265	110.2117	47.45402	156.0721	24358.5	0.854	0.73003
3	295	112.3924	51.61773	158.5162	25127.38	0.851	0.724072
4	310	120.6106	57.59967	172.3842	29716.33	0.821	0.674585
5	250	130.11	56.48403	188.0705	35370.53	0.782	0.611881

6	220	133.2254	56.72109	191.3338	36608.64	0.773	0.597776
7	340	137.2497	58.41737	195.3395	38157.5	0.762	0.580729

After considering the ranking of models (Without residuals), three DTAMD values emerge as the top performers. The first is the DTAMD 280° model, which outperforms all other models across all evaluation metrics, with the lowest values for MAE, MAPE, RMSE, MSE, and the highest values for R and R^2 (Table 2). The second-best performing model is the DTAMD 265°, which comes in at a close second to the top-ranked model with only slight variations in values for MAE, MAPE, RMSE, MSE, R and R^2 (Table 2). Finally, the DTAMD 295° model ranks third overall, performing better than the other models with DTAMD values of 220°, 250°, 310°, and 340° (Table 2). The use of rigorous evaluation metrics provides a precise analysis of the ranking of primary models. Furthermore, the change in the DTAMD angle values provides additional information about the impact of deviation of terrain aspect to the dominant moisture flux direction on model performance, and confirms the hypothesis of the existence of a rain shadow effect in mountainous areas.

Spatial Distribution and Factors Explanatory on Precipitation Patterns

The derived precipitation map (Fig. 4) exhibits an upward trend in precipitation with increasing altitude. Furthermore, our study reveals the presence of an orographic precipitation effect associated with a predominantly west-east oriented weather circulation pattern in Morocco, resulting in higher precipitation amounts on the western side of the Western and Central Rif, as well as the Middle and High Atlas, compared to the eastern side. These findings highlight the significant influence of high-latitude relief units on precipitation patterns.

In specific regions (Fig. 4), such as the western and Central Rif's western side at elevations ranging from 1,200 to 2,400 m, precipitation ranges from 1,000 to 1,700 mm, while the eastern side receives between 300 and 600 mm. Moving towards the south, the western side of the Middle Atlas (1500-3000 m) receives between 800 and 1100 mm, whereas the eastern side experiences precipitation between 150 and 400 mm. Further south, the western side of the High Atlas (2000-4000 m) receives precipitation ranging from 500 to 900 mm, while the eastern side receives between 50 and 250 mm. Additionally, smaller relief units with dimensions between 20 and 40 km also influence the spatial distribution of rainfall. These findings emphasize the significance of orographic effects and the existence of a rain shadow effect in the study area.

Moreover, the study reveals an exponential relationship between Latitude and precipitation (equation.2). Along the Atlantic coastline (Fig. 4), latitudes from 20° to 29° receive between 30 and 150 mm, mid-latitudes from 30° to 33° receive 200 to 400 mm, and high latitudes from 34° to 36° receive between 500 and 800 mm. Inland, these values can vary depending on the interaction between air masses and other influencing factors. The continentality effect is evident, with the coastal regions of the Chaouïa, Doukkala, and Abda plain receiving between 350 and 450 mm, whereas the R'hamna and Chiadma plateaus, along with the Al Haouz plain, experience precipitation ranging from 150 to 250 mm.

The analysis of precipitation spatial distribution in Morocco reveals a complex interplay of multiple factors that influence precipitation patterns. These factors include altitude, the scale of influence of relief on precipitation, orographic effects, the rain shadow effect, continentality, and Latitude. A comprehensive understanding of these dynamics is crucial for gaining deeper insights into the spatial distribution of rainfall and its intricate interactions with the environment.

Comparison between Module, Chelsa V2.1 and Worldclim V2

The evaluation of the final outcomes of the three models utilized for estimating the annual precipitation over Morocco was conducted and presented in Fig. 3. This assessment was based on a set of indicators and statistical efficiency factors, leveraging the data obtained from 53 stations that were excluded from the surface fitting and analysis, as outlined in Table 3. The examination of the outcomes led to the following conclusions:

The relative errors in the proposed model remain less than those obtained in other models. The analysis reveals that the proposed model exhibits deviations exceeding ±15% only for nine rain gauges, while Chelsa V2.1 and Worldclim V2 models demonstrate deviations in 27 and 23 rain gauges, respectively. Moreover, the proposed model indicates deviations exceeding ±5% in 28 rain gauges, whereas Chelsa V2.1 and Worldclim V2 models exhibit deviations in 10 and 16 rain gauges, respectively.

Table 3. Comparison of proposed Model using MAE, MAPE, RMSE, MSE, R and R^2 with annotation of the Chelsa V2.1 and the WorldClim V2 models

Models	MAE	MAPE	RMSE	MSE	R	R^2
Model proposed	9.060	1.971	32.633	1064.902	0.940	0.884
Chelsa V2.1	21.625	4.971	58.551	3428.215	0.854	0.729
WorldClim V2	15.607	3.586	43.244	1870.009	0.887	0.787

In general, it has been observed that relative errors are typically constrained between -10% and 10% in most domains (refer to Fig. 3 for a visual representation). No discernible predominant spatial pattern of error is evident. Nonetheless, it is notable that the most significant relative errors are situated in the Northern Middle Atlas region, which is characterized by elevated precipitation quantities and a dual influence of topographical factors. Moreover, a pervasive inclination towards overestimation is discernible in the eastern regions of the high Atlas and the southernmost sector of the country. Upon analyzing the generated maps, it is evident that the rain gauges exhibiting higher BIAS errors are concentrated in specific regions. Remarkably, the rain gauge situated in the valleys of mountainous regions, which is overestimated in all models, displays an error that can be attributed to a localized effect. This error is not influenced by precipitation resulting from sea winds but rather stems from the convective storms occurring in the region.

The results indicated that the "Model proposed" exhibited the best predictive ability. This model had lower MAE and MAPE values than the other two models, indicating a smaller average difference and the percentage difference between predicted and observed data. Furthermore, the "Model proposed" demonstrated higher levels of accuracy in predicting values, as indicated by its smallest RMSE and MSE values. Moreover, this model displayed a strong positive linear relationship between the predicted and observed data, as suggested by its high R and R^2 values (Table 3). Conversely, "Chelsa V2.1" displayed higher values of MAE, MAPE, RMSE, and MSE, and a weaker linear relationship between the predicted and observed values. Worldclim V2 showed moderate values of MAE, MAPE, RMSE, and MSE, as well as moderate values of R and R^2, signifying a moderate linear relationship between the predicted and actual values.

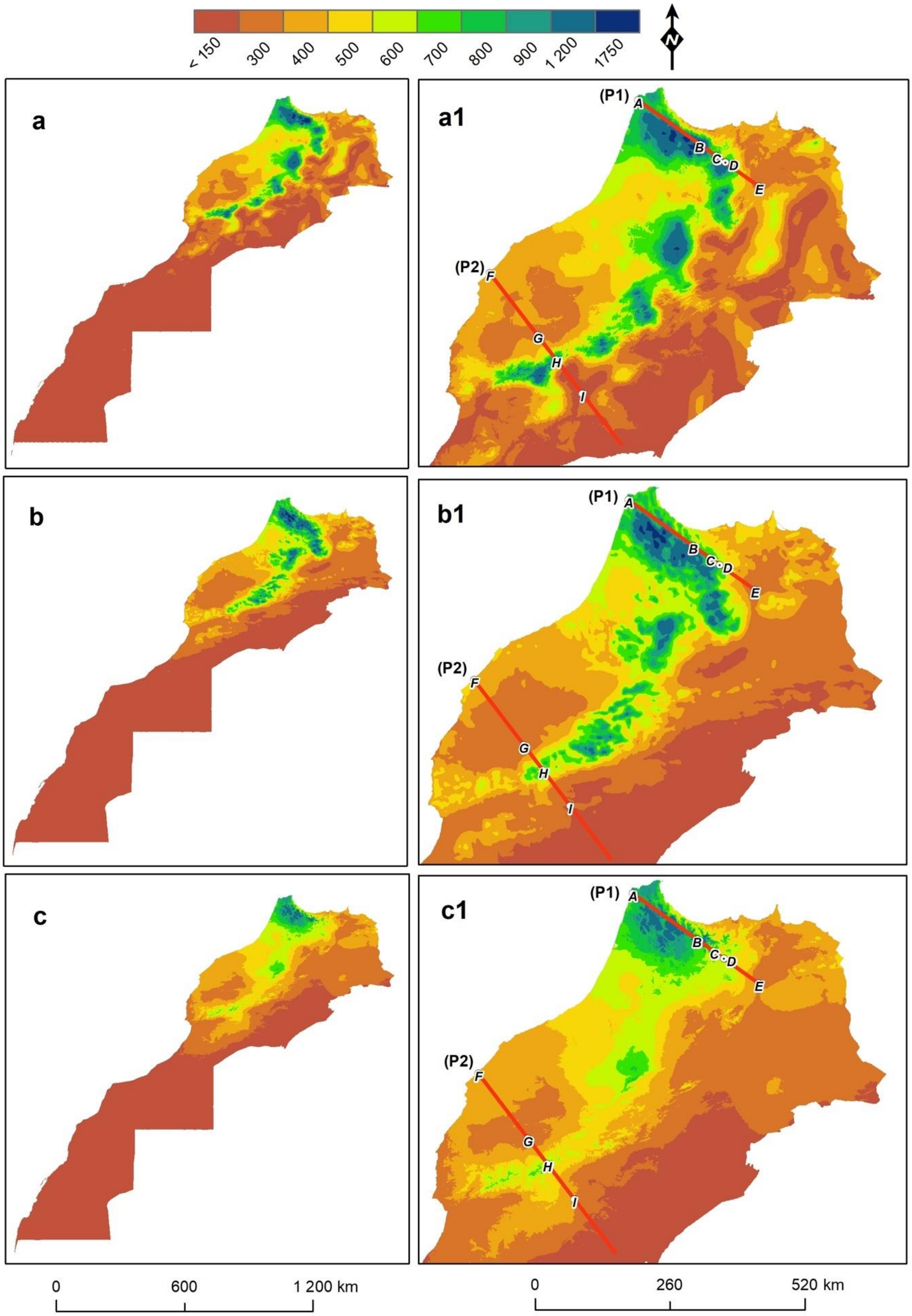

Figure 3. Estimation of the proposed model in comparison with the global surfaces of WorldClim V2 and CHELSA V2.1. over Morocco, with a focus on the Rif Mountains and Central of Morocco. The precipitation surface profiles (1) and (2). with an axis of northwest – southeast.

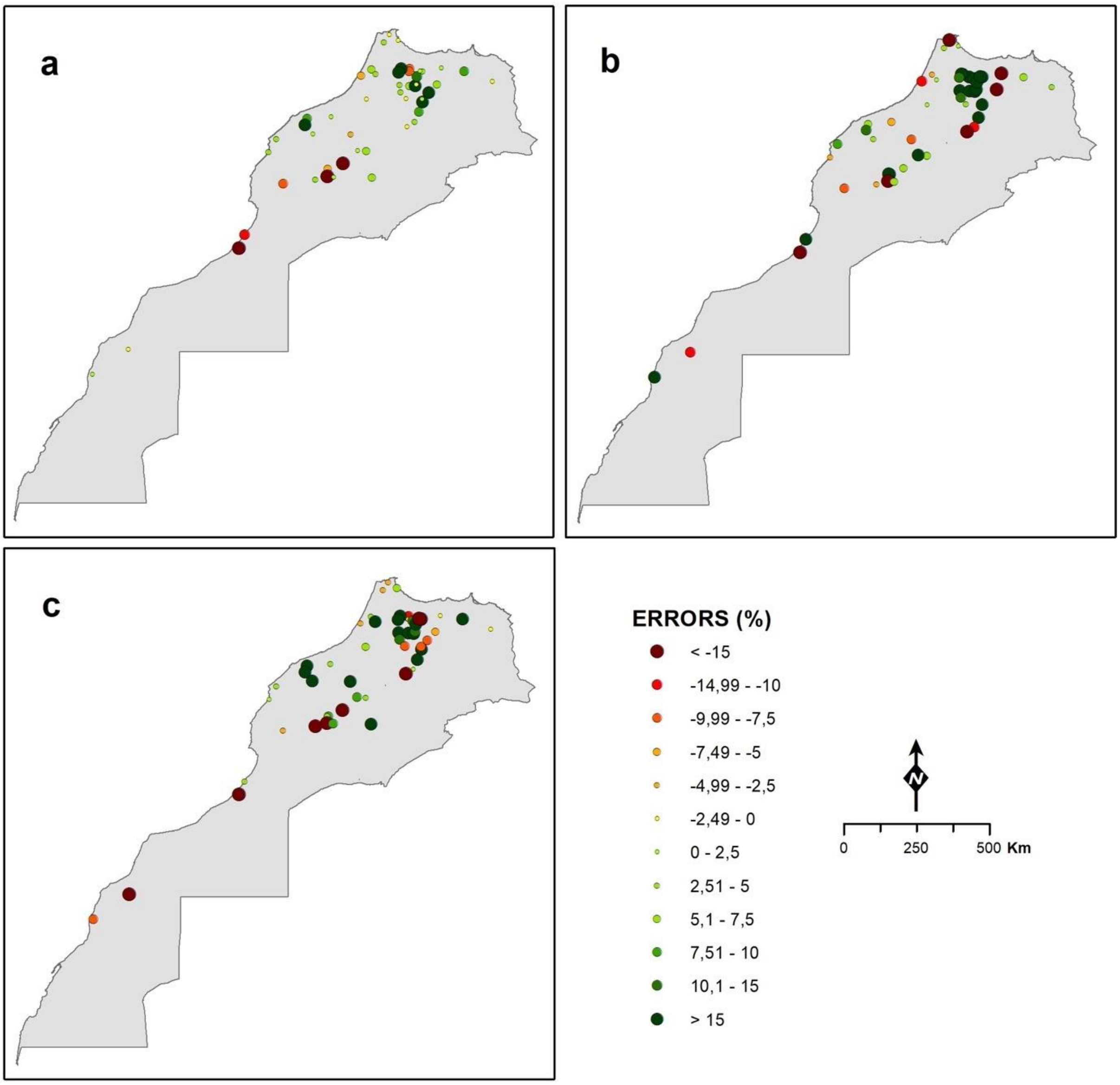

Figure 4. The Absolute Percentage Error Distribution was used to compare the performance of Module (a), Chelsa V2.1 (b), and WorldClim V2 (c) across 53 stations. These stations were not included in the modeling processes.

Upon examining Figure 5, which illustrate the spatial variation of precipitation in two profiles, we note that the proposed model demonstrates notable differences in precipitation estimates compared to the two global models. In the first profile (P1), which spans from the west of strait of Gibraltar, through the Rifaines chain, and ends on the plain of Guercif, the proposed model was more susceptible to orographic effects, resulting in a wetter estimation than the global models, particularly in the central and eastern areas of the Rif (truncating BC and CD, respectively). However, the models' annual precipitation estimates in the plains and hills were similar. In the second profile (P2), which extends from the south of the Doukala plain, through the Rehamna plateau (truncating FG) and the High Atlas, and ends on the Saharan lowlands and plains, the proposed model was less rainy in the areas located east of the High Atlas (truncating HI), and more so in the High Atlas Mountains than the global models. Nevertheless, the annual rainfall estimates in the vast areas of the Doukala plain and North of the Haouz Plain were similar among the three models where the decrease in precipitation was due to the continental effect.

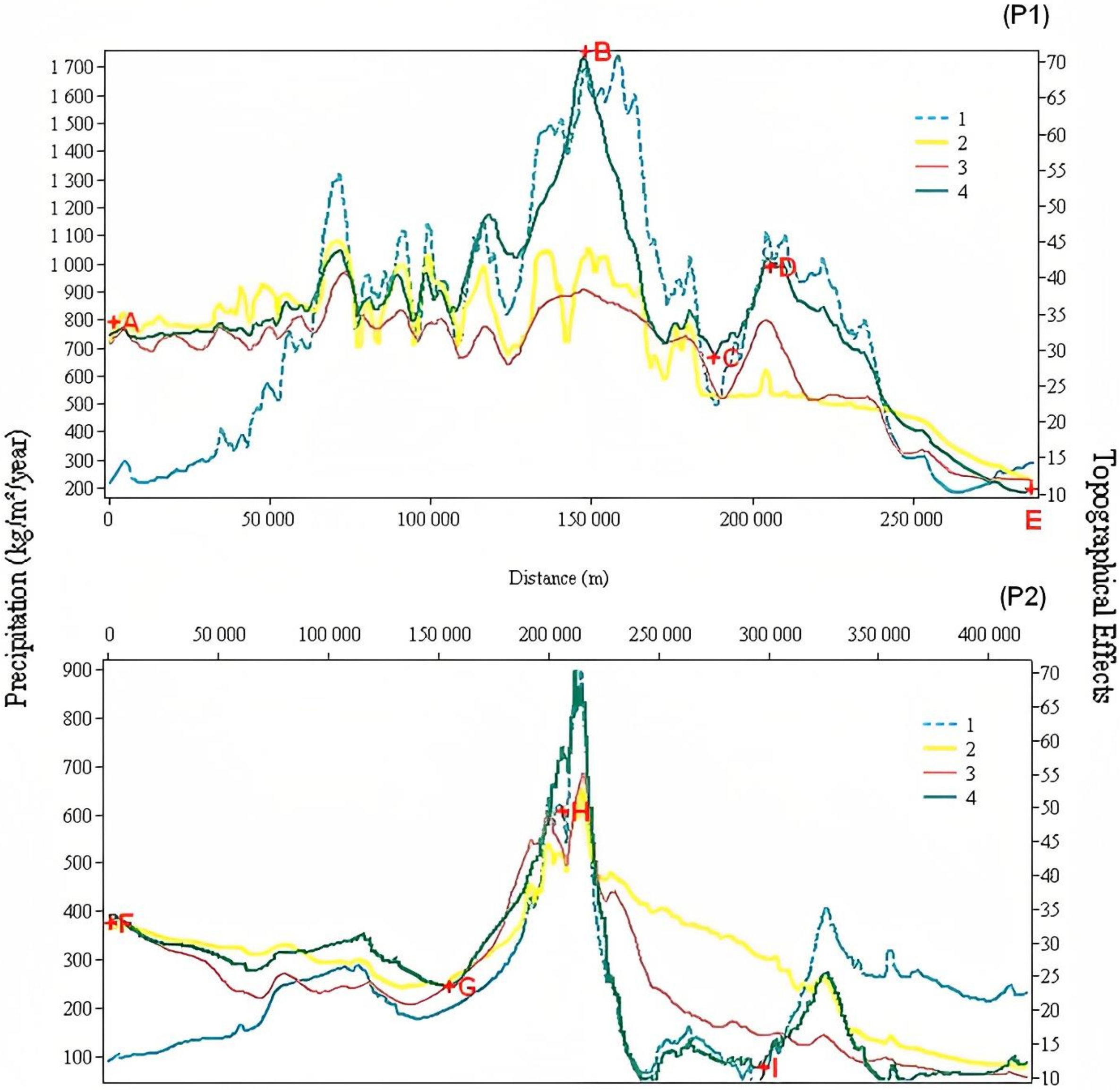

Figure 5. The difference between the proposed model compared to the global surface of CHELSA V2.1 and WorldClim V2 for annual precipitation Morocco. A, B, C, D, E, F, G, H, and I are the points of the precipitation surface profiles (P1) and (P2) (refer to Figure 3), with an axis of northwest - southeast.

Discussion and Conclusions

The proposed model uses various techniques and methodologies, including GIS tools, to examine the spatial patterns and fluctuations of precipitation. The model incorporates diverse variables, such as topography and geography, to elucidate the variations in precipitation. In addition, the distance from the coast, Latitude, terrain elevation, and the deviation of terrain aspect to the dominant moisture flux direction (DTAMD) were identified as the input variables that significantly influence precipitation mapping.

The model explicitly introduces the effects of these independent variables to enable automatic deduction by regression. To create the most precise DTAMD, a combination of standardized X, Y, Z1, Z2, and sin(s) maps were selected for every possible DTAMD, resulting in the highest determination coefficient. This approach facilitated the generation of a 45-year average annual precipitation map for Morocco, which was corrected for the inability of topographic and geographic variables to explain the complete spatial variation of precipitation. Among all models evaluated, the DTAMD 280° model emerged as the most optimal, exhibiting superior performance across all evaluation metrics, including the lowest values for MAE, MAPE, RMSE, MSE, and the highest values for R and R^2.

The use of explanatory factors alone is insufficient to determine the precipitation map. Therefore, our study employed spatial interpolation techniques to generate more accurate representations of rainfall patterns in Morocco. Specifically, we utilized the Idw technique to create residual surfaces during the spatial analysis of our proposed model. By combining these residual surfaces with the model surface, we were able to correct the limitations of topographic and geographic variables in explaining the complete spatial variation of precipitation. As depicted in Table 1, this approach resulted in a more precise 45-year average annual precipitation map for Morocco. Our method enabled us to understand Morocco's precipitation patterns better and improve our findings' accuracy.

The accuracy of global precipitation surfaces, such as those provided by CHELSA V2.1 and WorldClim V.2, is comparatively lower when compared to the proposed model. Therefore, utilizing the local surface for hydrological and environmental assessments is more appropriate. This locally derived surface serves as a reliable foundation for representing the precipitation patterns from 1965 to 2010. Moreover, it can be effectively utilized as input data for climate change models and projections. By incorporating this locally derived surface, a more accurate and comprehensive understanding of precipitation dynamics can be achieved in various regions of interest.

In interpreting the spatial variation of precipitation in northern Morocco, particularly in the Rif Mountains, Middle Atlas, and high plateaus, two essential factors play a significant role: the orographic effect and distance from the coast. Their influence was comparatively less prominent in central Morocco, especially in the High Atlas and Anti-Atlas, and gradually decreased as we proceeded towards the southern regions. The impact of the distance from the coast was evident on the Atlantic plains and the R'hamna and Chiadma plateaus. This is because ocean currents and sea surface temperatures can modify the temperature and moisture content of the overlying air masses, which, in turn, affects precipitation patterns. Regarding the impact of Latitude, it was found to have an exponential effect, with precipitation increasing from south to North. The amount of precipitation decreased from lower latitudes (20 degrees) in the southern regions towards higher latitudes (36 degrees) in the northern regions due to reduced solar radiation received at higher latitudes, leading to lower atmospheric instability and less frequent convective activity.

The generated precipitation map for Morocco demonstrated that the northern regions, particularly the Rif mountain range, received the highest precipitation amounts, while the southern regions, including the Sahara Desert, received the least precipitation. The coastal regions along the North Atlantic Ocean exhibited relatively high precipitation amounts, while the mountainous regions of the High Atlas and Anti-Atlas ranges displayed moderate precipitation amounts due to the orographic lifting effect.

In general, the proposed approach can be utilized to accurately estimate the annual precipitation amounts in Morocco, which can have important implications for water resource management, agriculture, and urban planning. The approach can also be applied to other regions with similar topographic and geographic characteristics to estimate precipitation amounts and provide insights into the impact of climate change on precipitation patterns. However, it is important to note that the proposed approach is limited to analyzing annual precipitation amounts and may not accurately estimate precipitation amounts for shorter periods or extreme weather events.

In conclusion, the proposed model provides a useful tool for estimating the annual precipitation amounts in Morocco and can be utilized by policymakers, researchers, and other stakeholders to make informed decisions related to water resource management, agriculture, and urban planning. Further research is needed to evaluate the performance of the proposed model in other regions and to improve its accuracy for extreme weather events.

Acknowledgments

The authors are grateful for the data support provided by the Hydraulic Basin Agencies and the National Meteorological Directorate.

Data Availability Statement

GDEM dataset is available in https://asterweb.jpl.nasa.gov and the historical climate data is available in https://chelsa-climate.org and https://www.worldclim.com.

Conflicts of Interest

The authors declare no conflicts of interest.

References

AAD. (2015). *Investor's guide in the agricultural sector in Morocco*. Rabat Retrieved from www.agriculture.gov.ma

Alsafadi, K., Mohammed, S., Mokhtar, A., Sharaf, M., & He, H. (2021). Fine-resolution precipitation mapping over Syria using local regression and spatial interpolation. *Atmospheric Research, 256*, 105524.

Barbulescu, A. (2016). A New Method for Estimation the Regional Precipitation. *Water Resources Management, 30*(1), 33-42. https://doi.org/10.1007/s11269-015-1152-2

Basist, A., Bell, G. D., & Meentemeyer, V. (1994). Statistical relationships between topography and precipitation patterns. *Journal of climate, 7*(9), 1305-1315.

Beck, H. E., Pan, M., Roy, T., Weedon, G. P., Pappenberger, F., Van Dijk, A. I., . . . Wood, E. F. (2019). Daily evaluation of 26 precipitation datasets using Stage-IV gauge-radar data for the CONUS. *Hydrology and Earth System Sciences, 23*(1), 207-224.

Benabid, A. (2000). Flore et écosystèmes du Maroc: Evaluation et préservation de la biodiversité.

Benyoussef, S., Arabi, M., El Yousfi, Y., Ben Cheikh, B., Abdaoui, A., Azirar, M., . . . Ait Boughrous, A. (2024). Climate Change and Water Resources Management in Ghis-Nekor Watershed (North of Morocco) – A Comprehensive Analysis Using SPI, RDI and DI Indices. *Ecological Engineering & Environmental Technology, 25*(2), 199-209. https://doi.org/10.12912/27197050/176275

Bookhagen, B., & Strecker, M. R. (2008). Orographic barriers, high-resolution TRMM rainfall, and relief variations along the eastern Andes. *Geophysical Research Letters, 35*(6).

Bostan, P. A., Heuvelink, G. B. M., & Akyurek, S. Z. (2012). Comparison of regression and kriging techniques for mapping the average annual precipitation of Turkey. *International Journal of Applied Earth Observation and Geoinformation, 19*, 115-126. https://doi.org/10.1016/j.jag.2012.04.010

Camera, C., Bruggeman, A., Hadjinicolaou, P., Michaelides, S., & Lange, M. A. (2017). Evaluation of a spatial rainfall generator for generating high resolution precipitation projections over orographically complex terrain. *Stochastic Environmental Research and Risk Assessment, 31*(3), 757-773. https://doi.org/10.1007/s00477-016-1239-1

Chang, T. J. (1991). Investigation of precipitation droughts by use of kriging method. *Journal of Irrigation and Drainage Engineering, 117*(6), 935-943.

Chanyour, Y., El Achari, O., Hanchane, M., Obda, K., & Kessabi, R. (2024). Monthly and Annual Precipitation in Arid Environment of the Daoura Watershed (South-Eastern

Morocco) – Homogenization and Trend Analysis. *Ecological Engineering & Environmental Technology, 25*(4), 125-142. https://doi.org/10.12912/27197050/178530

Crochet, P., Jóhannesson, T., Jónsson, T., Sigurðsson, O., Björnsson, H., Pálsson, F., & Barstad, I. (2007). Estimating the spatial distribution of precipitation in Iceland using a linear model of orographic precipitation. *Journal of Hydrometeorology, 8*(6), 1285-1306.

Daly, C., Halbleib, M., Smith, J. I., Gibson, W. P., Doggett, M. K., Taylor, G. H., . . . Pasteris, P. P. (2008). Physiographically sensitive mapping of climatological temperature and precipitation across the conterminous United States. *International Journal of Climatology: a Journal of the Royal Meteorological Society, 28*(15), 2031-2064.

Daly, C., Neilson, R. P., & Phillips, D. L. (1994). A statistical-topographic model for mapping climatological precipitation over mountainous terrain. *Journal of Applied Meteorology and Climatology, 33*(2), 140-158.

Daly, C., Slater, M. E., Roberti, J. A., Laseter, S. H., & Swift Jr, L. W. (2017). High-resolution precipitation mapping in a mountainous watershed: ground truth for evaluating uncertainty in a national precipitation dataset. *International Journal of Climatology, 37*, 124-137.

Daly, C., Taylor, G., & Gibson, W. (1997). *The PRISM approach to mapping precipitation and temperature.* Paper presented at the Proc., 10th AMS Conf. on Applied Climatology.

Danard, M. (1976). On frictional and orographic effects on precipitation in coastal areas. *Boundary-Layer Meteorology, 10*(4), 409-422.

Di Piazza, A., Conti, F. L., Noto, L. V., Viola, F., & La Loggia, G. (2011). Comparative analysis of different techniques for spatial interpolation of rainfall data to create a serially complete monthly time series of precipitation for Sicily, Italy. *International Journal of Applied Earth Observation and Geoinformation, 13*(3), 396-408. doi:https://doi.org/10.1016/j.jag.2011.01.005

Diodato, N., & Ceccarelli, M. (2005). Interpolation processes using multivariate geostatistics for mapping of climatological precipitation mean in the Sannio Mountains (southern Italy). *Earth Surface Processes and Landforms: The Journal of the British Geomorphological Research Group, 30*(3), 259-268.

Du, Y., Wang, D., Zhu, J., Lin, Z., & Zhong, Y. (2022). Intercomparison of multiple high-resolution precipitation products over China: Climatology and extremes. *Atmospheric Research, 278*, 106342. https://doi.org/10.1016/j.atmosres.2022.106342

Fick, S. E., & Hijmans, R. J. (2017). WorldClim 2: new 1-km spatial resolution climate surfaces for global land areas. *International Journal of Climatology, 37*(12), 4302-4315.

Fu, S., Sonnenborg, T. O., Jensen, K. H., & He, X. (2011). Impact of precipitation spatial resolution on the hydrological response of an integrated distributed water resources model. *Vadose Zone Journal, 10*(1), 25-36.

Gilewski, P. (2021). Impact of the grid resolution and deterministic interpolation of precipitation on rainfall-runoff modeling in a sparsely gauged mountainous catchment. *Water, 13*(2), 230.

Giovanis, E., & Ozdamar, O. (2022). The impact of climate change on budget balances and debt in the Middle East and North Africa (MENA) region. *Climatic Change, 172*(3), 34. https://doi.org/10.1007/s10584-022-03388-x

Guan, H., Wilson, J. L., & Makhnin, O. (2005). Geostatistical mapping of mountain precipitation incorporating autosearched effects of terrain and climatic characteristics. *Journal of Hydrometeorology, 6*(6), 1018-1031.

Gundogdu, I. B. (2017). Usage of multivariate geostatistics in interpolation processes for meteorological precipitation maps. *Theoretical and Applied Climatology, 127*, 81-86.

Hofierka, J., Parajka, J., Mitasova, H., & Mitas, L. (2002). Multivariate interpolation of precipitation using regularized spline with tension. *Transactions in GIS, 6*(2), 135-150.

Jeniffer, K., Su, Z., Woldai, T., & Maathuis, B. (2010). Estimation of spatial–temporal rainfall distribution using remote sensing techniques: A case study of Makanya catchment, Tanzania. *International Journal of Applied Earth Observation and Geoinformation, 12*, S90-S99. https://doi.org/10.1016/j.jag.2009.10.003

Jeong, H.-G., Ahn, J.-B., Lee, J., Shim, K.-M., & Jung, M.-P. (2020). Improvement of daily precipitation estimations using PRISM with inverse-distance weighting. *Theoretical and Applied Climatology, 139*, 923-934.

Jin, H., Chen, X., Wu, P., Song, C., & Xia, W. (2021). Evaluation of spatial-temporal distribution of precipitation in mainland China by statistic and clustering methods. *Atmospheric Research, 262*, 105772. https://doi.org/10.1016/j.atmosres.2021.105772

Karger, D. N., Conrad, O., Böhner, J., Kawohl, T., Kreft, H., Soria-Auza, R. W., . . . Kessler, M. (2017). Climatologies at high resolution for the earth's land surface areas. *Scientific data, 4*(1), 1-20.

Lloyd, C. (2005). Assessing the effect of integrating elevation data into the estimation of monthly precipitation in Great Britain. *Journal of Hydrology, 308*(1-4), 128-150.

Lloyd, C. D. (2010). Multivariate interpolation of monthly precipitation amount in the United Kingdom. *geoENV VII–geostatistics for environmental applications*, 27-39.

Ly, S., Charles, C., & Degré, A. (2013). Different methods for spatial interpolation of rainfall data for operational hydrology and hydrological modeling at watershed scale: a review. *Biotechnologie, agronomie, société et environnement, 17*(2).

Meersmans, J., Van Weverberg, K., De Baets, S., De Ridder, F., Palmer, S., Van Wesemael, B., & Quine, T. (2016). Mapping mean total annual precipitation in Belgium, by investigating the scale of topographic control at the regional scale. *Journal of Hydrology, 540*, 96-105.

Mirás-Avalos, J. M., Mestas-Valero, R. M., Sande-Fouz, P., & Paz-González, A. (2009). Consistency analysis of pluviometric information in Galicia (NW Spain). *Atmospheric Research, 94*(4), 629-640.

Ninyerola, M., Pons, X., & Roure, J. M. (2007). Monthly precipitation mapping of the Iberian Peninsula using spatial interpolation tools implemented in a Geographic Information System. *Theoretical and Applied Climatology, 89*, 195-209.

Okacha, A., Salhi, A., Arari, K., Elbadaou, K., & Lahrichi, K. (2023). Soil erosion assessment using the RUSLE model for better planning: a case study from Morocco. *Modeling Earth Systems and Environment*, 1-9.

Ouharba, E. H., Mabrouki, J., & Triqui, Z. E. A. (2024). Assessment and Future Climate Dynamics in the Bouregreg Basin, Morocco - Impacts and Adaptation Alternatives. *Ecological Engineering & Environmental Technology, 25*(3), 51-63. https://doi.org/10.12912/27197050/177823

Pichura, V., Potravka, L., & Barulina, I. (2023). Agricultural Dependence of the Formation of Water Balance Stability of the Sluch River Basin Under Conditions of Climate Change. *Ecological Engineering & Environmental Technology, 24*(9), 300-325. https://doi.org/10.12912/27197050/174163

Prakash, S. (2019). Performance assessment of CHIRPS, MSWEP, SM2RAIN-CCI, and TMPA precipitation products across India. *Journal of Hydrology, 571*, 50-59. https://doi.org/10.1016/j.jhydrol.2019.01.036

Salhi, A., Benabdelouahab, T., Martin-Vide, J., Okacha, A., El Hasnaoui, Y., El Mousaoui, M., . . . Lebrini, Y. (2020). Bridging the gap of perception is the only way to align soil protection actions. *Science of the Total Environment, 718*, 137421.

Salhi, A., Martin-Vide, J., Benhamrouche, A., Benabdelouahab, S., Himi, M., Benabdelouahab, T., & Casas Ponsati, A. (2019). Rainfall distribution and trends of the daily precipitation concentration index in northern Morocco: a need for an adaptive environmental policy. *SN Applied Sciences*, *1*, 1-15.

Salhi, A., Vila Subirós, J., & Insalaco, E. (2022). Spatial patterns of environmental degradation and demographic changes in the Mediterranean fringes. *Geocarto International*, 1-17. https://doi.org/10.1080/10106049.2022.2090619

Seo, Y., Kim, S., & Singh, V. P. (2015). Estimating spatial precipitation using regression kriging and artificial neural network residual kriging (RKNNRK) hybrid approach. *Water Resources Management, 29*, 2189-2204.

SHU, S. J., WANG, Y., & XIONG, A. Y. (2007). Estimation and analysis for geographic and orographic influences on precipitation distribution in China. *Chinese Journal of Geophysics, 50*(6), 1482-1493.

Symeonakis, E., Bonifaçio, R., & Drake, N. (2009). A comparison of rainfall estimation techniques for sub-Saharan Africa. *International Journal of Applied Earth Observation and Geoinformation, 11*(1), 15-26. https://doi.org/10.1016/j.jag.2008.04.002

Tachikawa, T., Kaku, M., Iwasaki, A., Gesch, D. B., Oimoen, M. J., Zhang, Z., . . . Carabajal, C. (2011). *ASTER Global Digital Elevation Model Version 2 - summary of validation results*. Retrieved from http://pubs.er.usgs.gov/publication/70005960

Tan, J., Xie, X., Zuo, J., Xing, X., Liu, B., Xia, Q., & Zhang, Y. (2021). Coupling random forest and inverse distance weighting to generate climate surfaces of precipitation and temperature with multiple-covariates. *Journal of Hydrology, 598*, 126270.

Verdin, A., Rajagopalan, B., Kleiber, W., & Funk, C. (2015). AB ayesian kriging approach for blending satellite and ground precipitation observations. *Water Resources Research, 51*(2), 908-921.

Vidal P, I., & Varas, E. (1982). Rainfall estimation in places without data. *Agricultura Tecnica (Chile)*.

Waha, K., Krummenauer, L., Adams, S., Aich, V., Baarsch, F., Coumou, D., . . . Schleussner, C.-F. (2017). Climate change impacts in the Middle East and Northern Africa (MENA) region and their implications for vulnerable population groups. *Regional Environmental Change, 17*(6), 1623-1638. https://doi.org/10.1007/s10113-017-1144-2

Wang, S., Huang, G., Lin, Q., Li, Z., Zhang, H., & Fan, Y. (2014). Comparison of interpolation methods for estimating spatial distribution of precipitation in Ontario, Canada. *International Journal of Climatology, 34*(14), 3745-3751.

Wei, C., Dong, X., Ma, Y., Gou, J., Li, L., Bo, H., . . . Su, B. (2023). Applicability comparison of various precipitation products of long-term hydrological simulations and their impact on parameter sensitivity. *Journal of Hydrology, 618*, 129187. https://doi.org/10.1016/j.jhydrol.2023.129187